

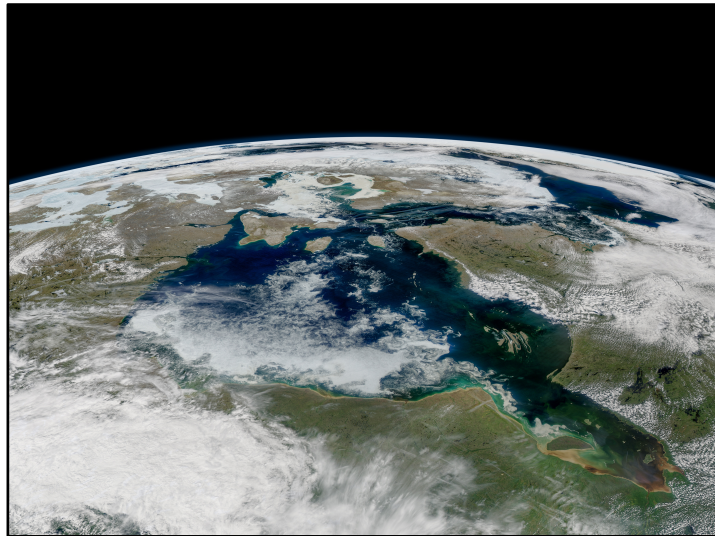


vEGU21

Gather Online | 19–30 April 2021



THERMOCHEMICAL STRUCTURE OF THE SUPERIOR CRATON FROM MULTI-OBSERVABLE PROBABILISTIC INVERSION

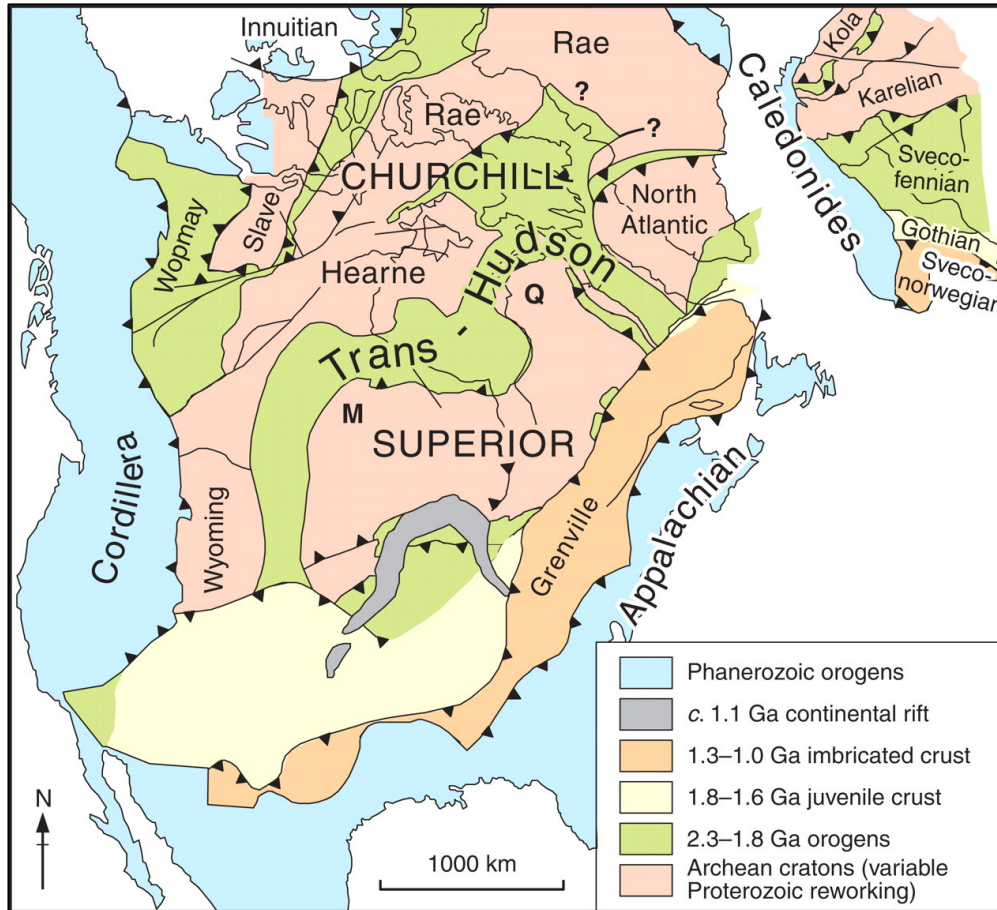


Riddhi Dave



DE BEERS GROUP

Geological Map



- ❖ Superior craton: largest and best preserved Archean craton, assembled by 2.5 Ga
- ❖ Assembly of Laurentia via orogenesis throughout the Proterozoic
- ❖ Closure of Rheic and Iapetus Oceans during the Phanerozoic
- ❖ Double-indentor shape of the Superior craton → likely entrapment of juvenile material in the Trans-Hudson Orogen

[Modified from *Hoffman, 1988*]

An Interesting Problem

- ❖ The thermochemical structure of the lithosphere is a key factor in modulating or controlling surface processes
- ❖ Reliable estimates of the 3-D temperature distribution and compositional structure beneath continents are difficult to obtain and surrounded by methodological controversy

Questions:

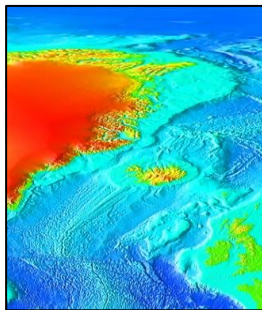
- (i) How can we obtain reliable models of the first-order thermochemical structure of the lithosphere?
- (ii) To what extent are different tectonic models and processes actually supported or required by independent geophysical, geological, and geochemical evidence?
- (iii) How can we combine multiple observations with complementary sensitivities into a thermodynamically and internally consistent framework?

Answer:

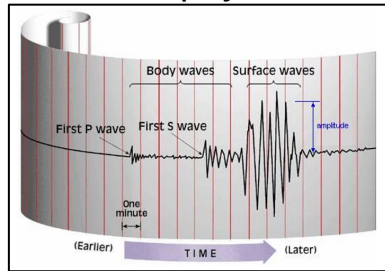
Multi-observable probabilistic tomography

Integrating Geological and Geophysical Data

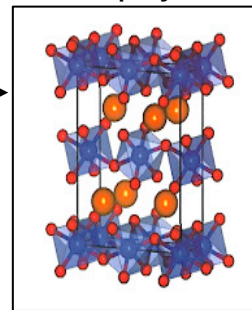
Surface Observables



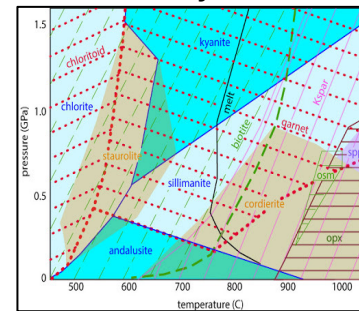
Geophysics



Mineral physics



Thermodynamics

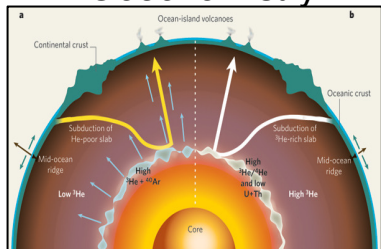


Probabilistic, Multi-Observable, Internally-Consistent Inverse Framework

Petrology and mineralogy

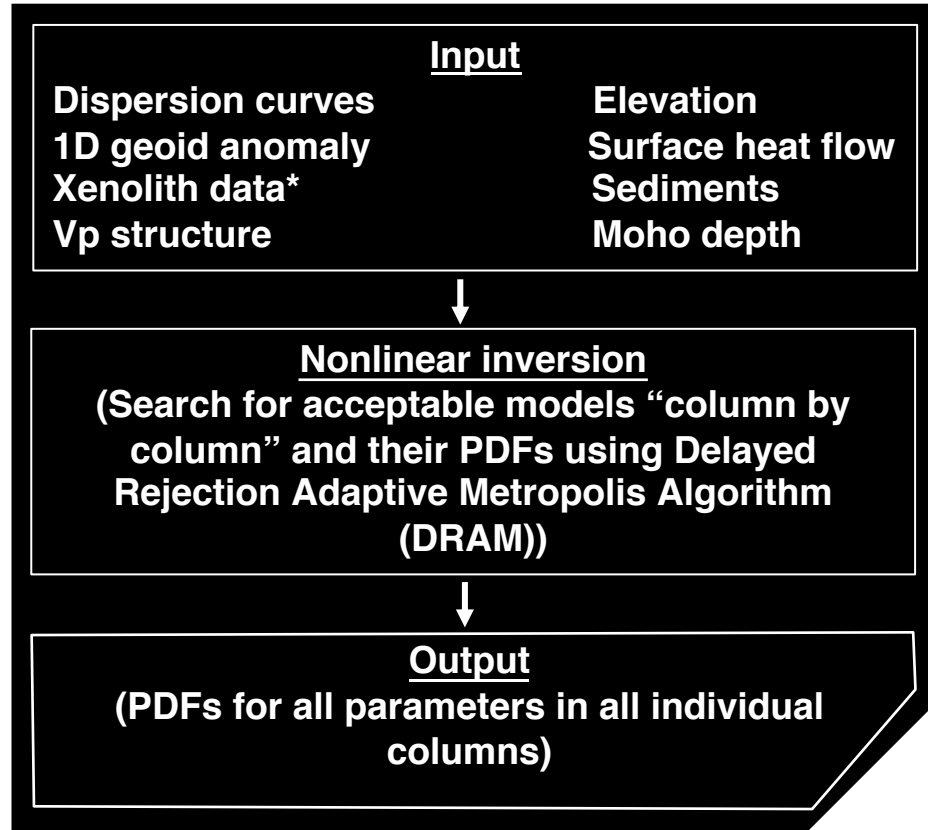


Geochemistry



How is it done?

First Part (MC search in 1-D)

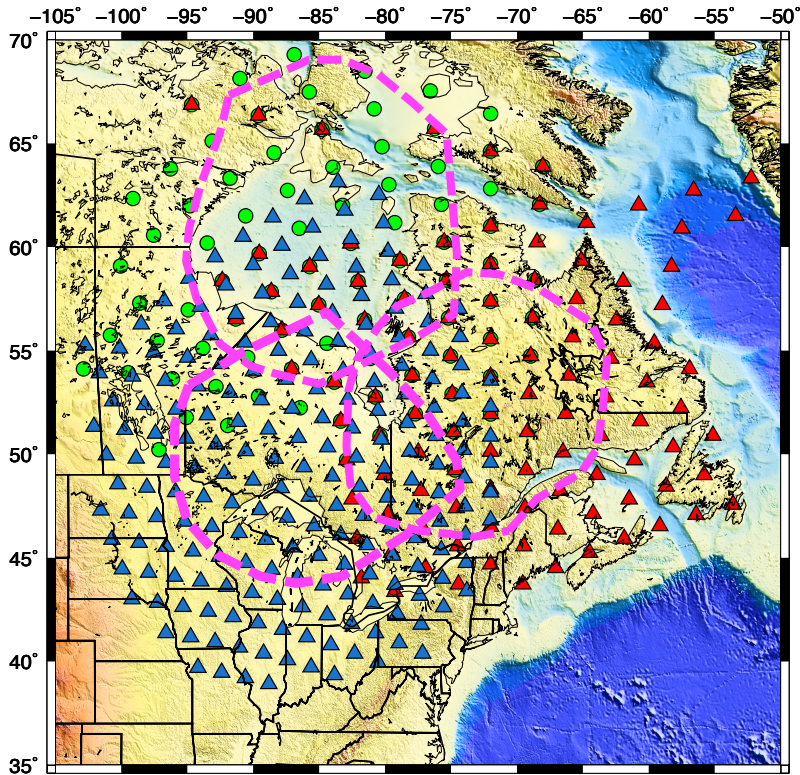


Posterior PDF: In a Bayesian framework, the solution to the inverse problem is given by the Posterior Probability Density Function (PDF), which contains the ensemble of acceptable models as allowed by data and a prior information.

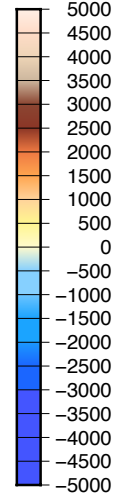
Second Part
(refinement in 3-D)

*From global petrological database- When this information is reliable, it serves as a priori constraints

Surface Wave (Rayleigh Wave) Tomography



meters

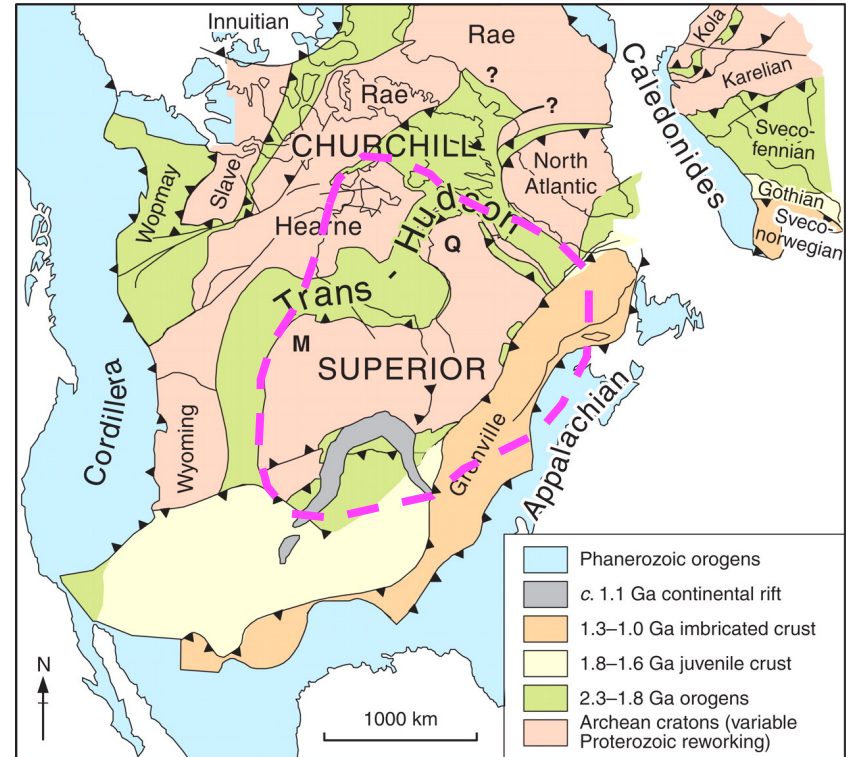


▲ Foster et al., 2020

▲ Petrescu et al., 2017

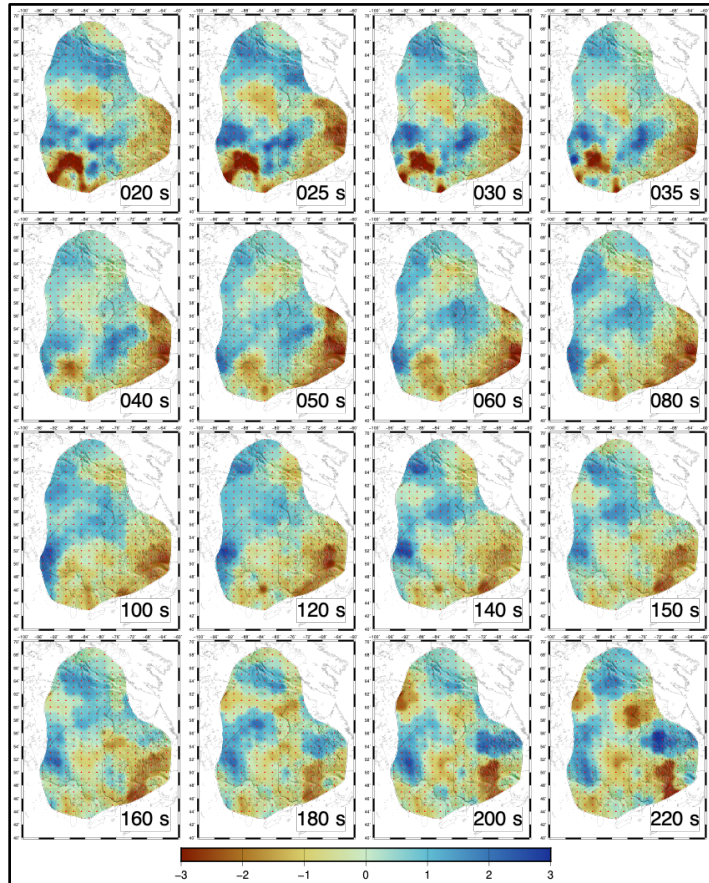
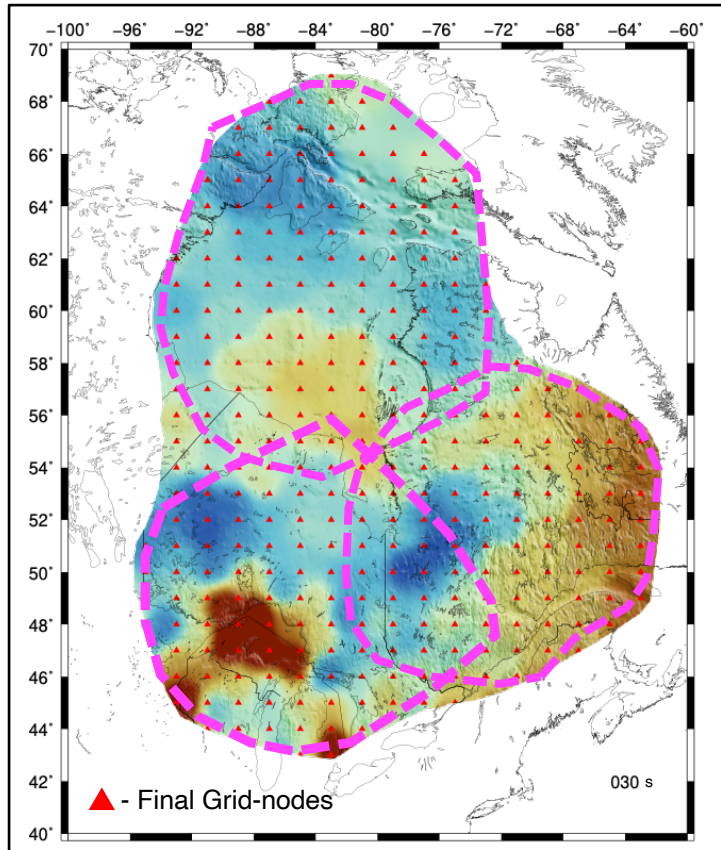
● Darbyshire et al., 2013

— Best-resolved zone for each study



[Modified from Hoffman, 1988]

Composite Phase Velocity Maps



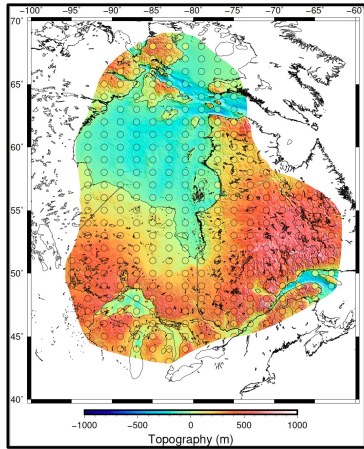
Phase velocity anomaly (%)

Data and Data processing steps:

- ❖ Shortest 20 s to the longest 220 s
- ❖ Clipping of each data-set based on ray-path coverage and resolution
- ❖ Weighted-average of regions of overlap
- ❖ Interpolating and gridding
- ❖ 312 Grid-nodes

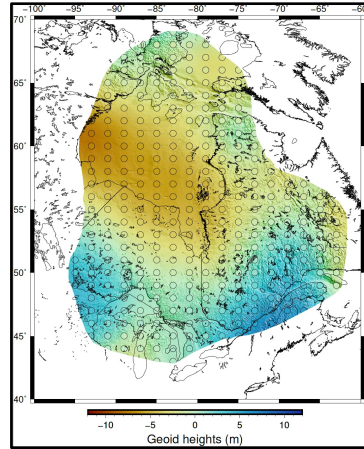
Surface Observables

Topography



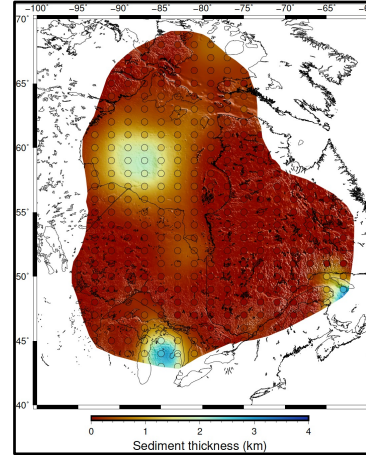
Etopo1

Geoid anomaly



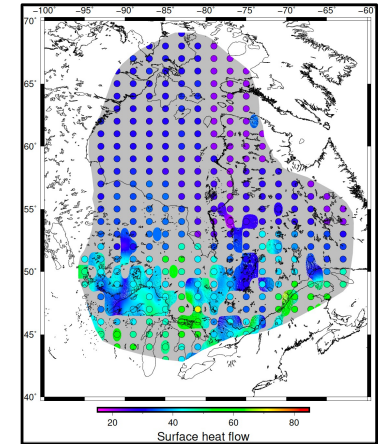
EGM2008

Sediment thickness



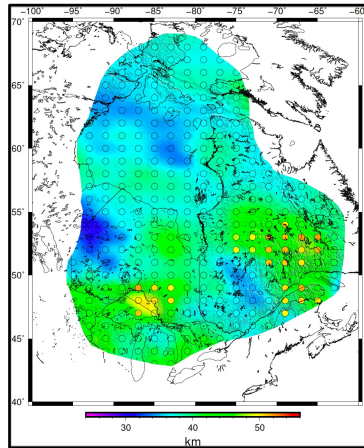
Crust1.0

Surface heat flow



*-Mareschal
-Pers. comm.*

Moho Depth

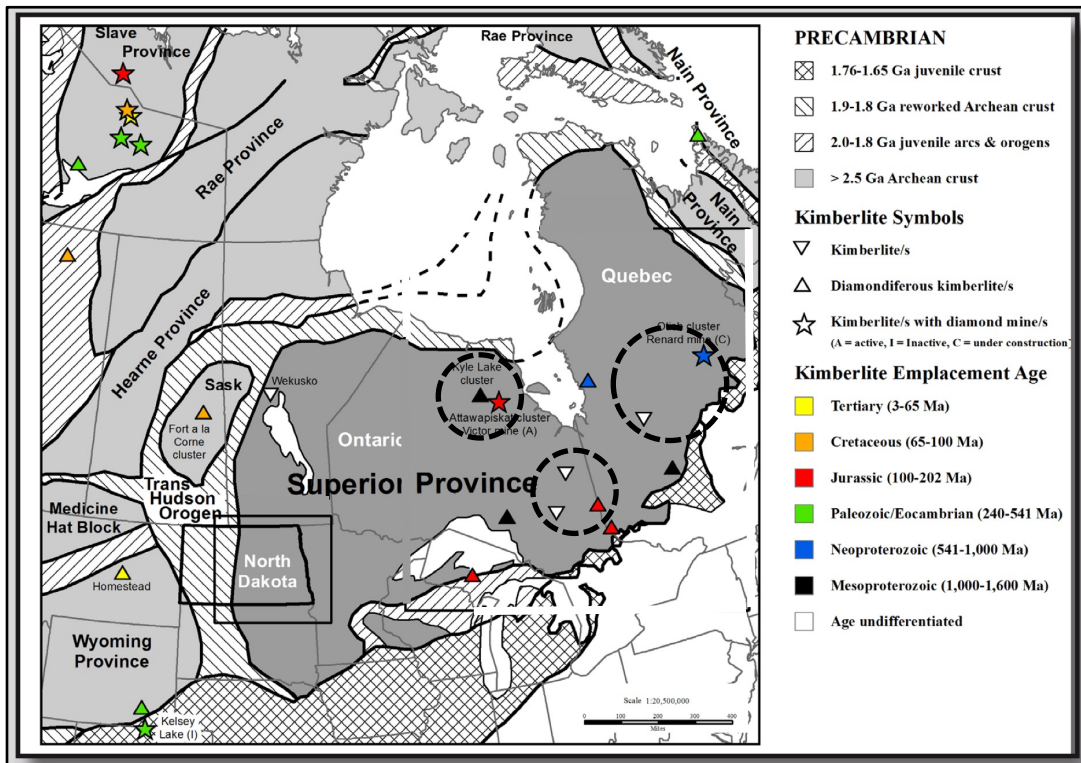


- CRUST1.0* Laske et al., 2013
- Tesauro et al.*, 2014
- Shen & Ritzwoller*, 2016
- LITHOPROBE*
- Receiver function studies*

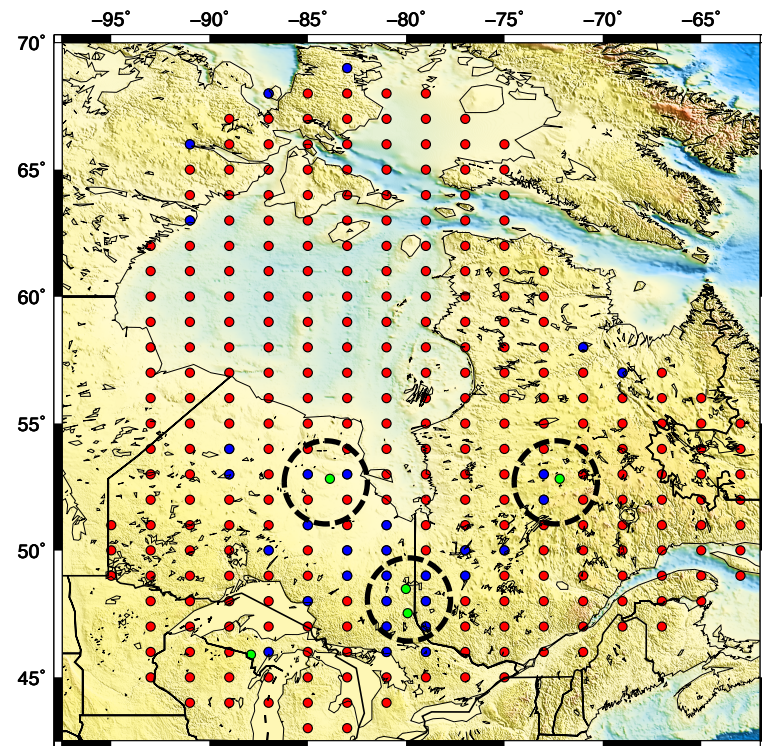
Other Geophysical Inputs :

- Body wave data
(*BBNAP19: Boyce et al.*, 2019)
- Global tomography model
(*GYPSUM: Simmons et al.*, 2010)

Tectonic Map with Kimberlites

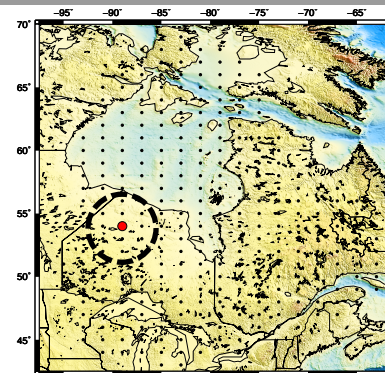
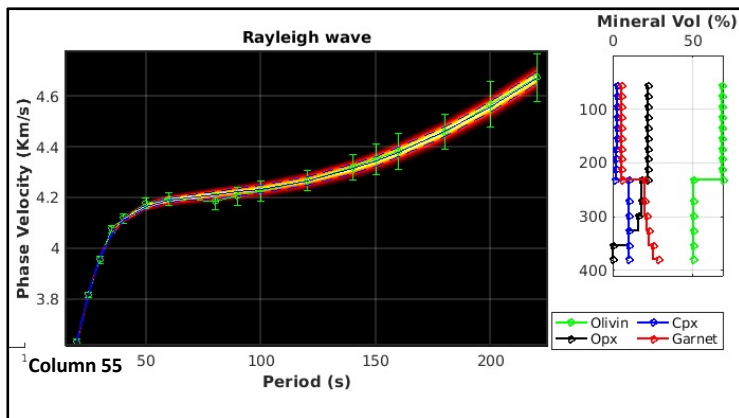
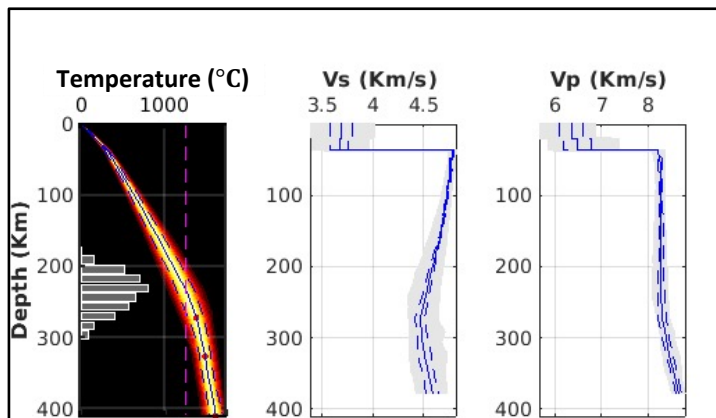


[Nesheim, 2016]

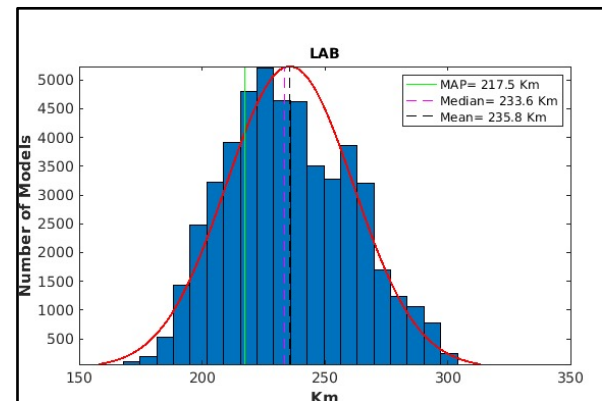
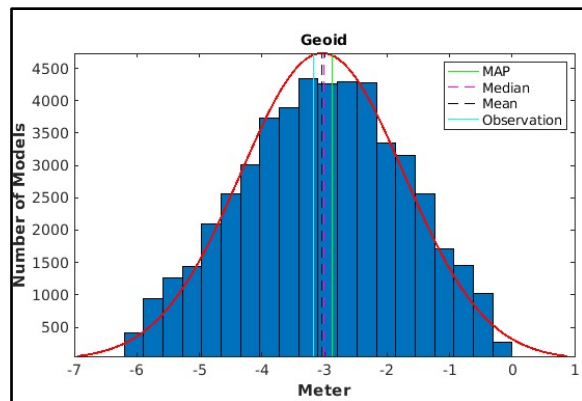
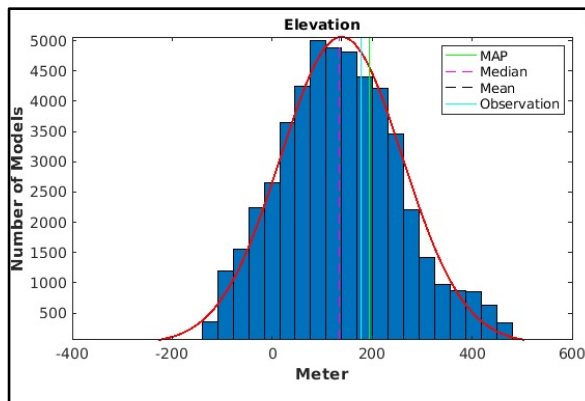


- - Uniformly spaced Grid nodes
- - Grid nodes on known kimberlite clusters
- - Grid nodes outside uniform spacing

1D Outputs – Column 55



❖ 1000s of accepted models; histograms show most likely values & uncertainties

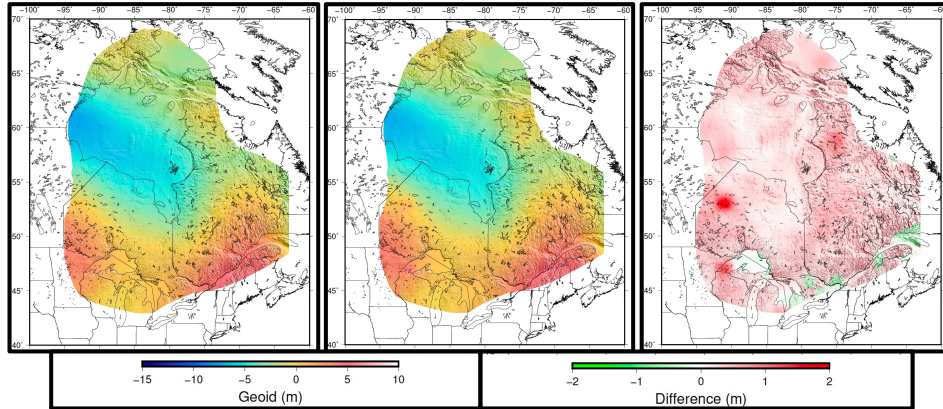


Geoid, Surface heat flow, and Topography

Observed

Predicted

Difference

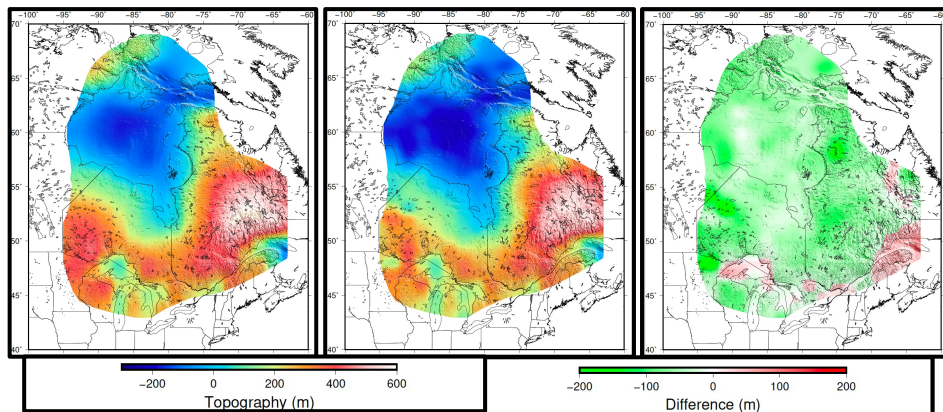


- ❖ Predicted data are depicted as the means of their respective posterior PDFs
- ❖ The fit to dispersion data remains within uncertainties in most of the study area
- ❖ Both predicted geoid and elevation fit closely the observed values within their assigned uncertainties

Observed

Predicted

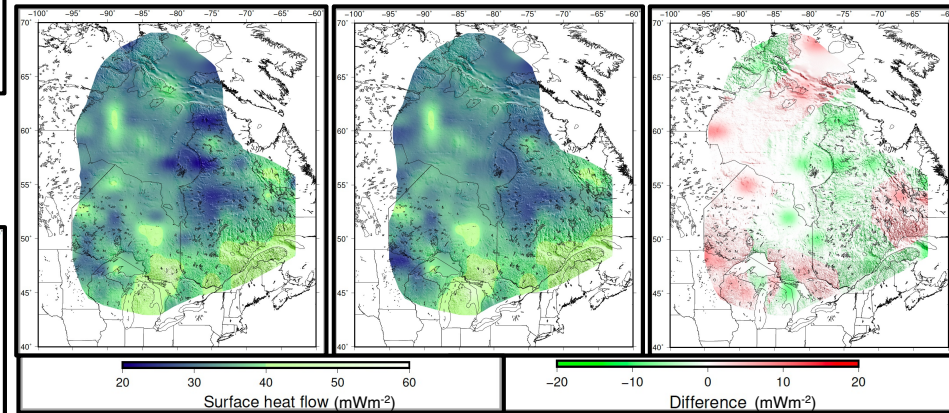
Difference



Observed

Predicted

Difference



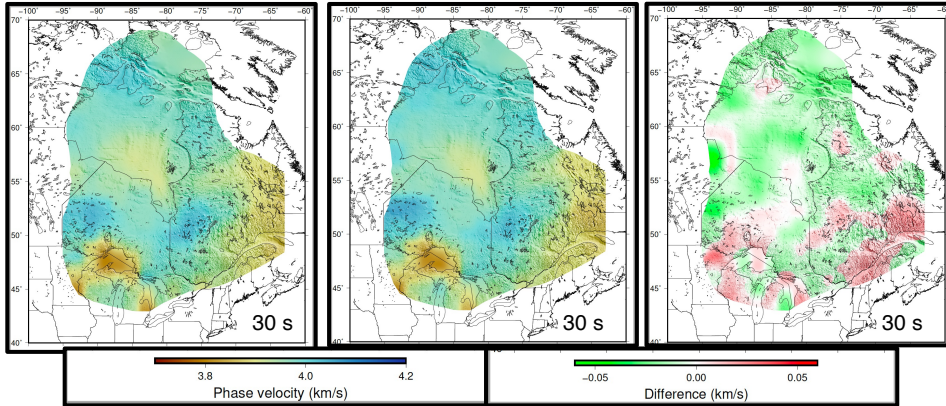
- ❖ The predicted SHF data shows an average value of $\sim 40 \text{ mWm}^{-2}$
- ❖ Differences between observed and predicted are within the assumed uncertainty of $\pm 15 \text{ mWm}^{-2}$

Phase Velocities

Observed

Predicted

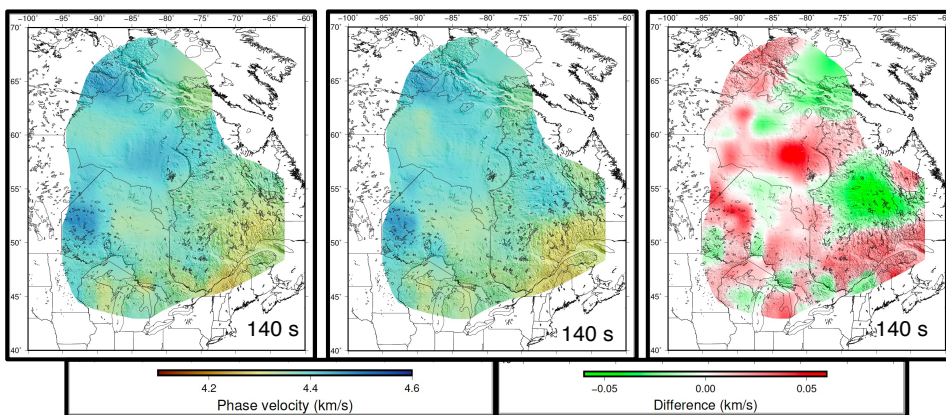
Difference



Observed

Predicted

Difference

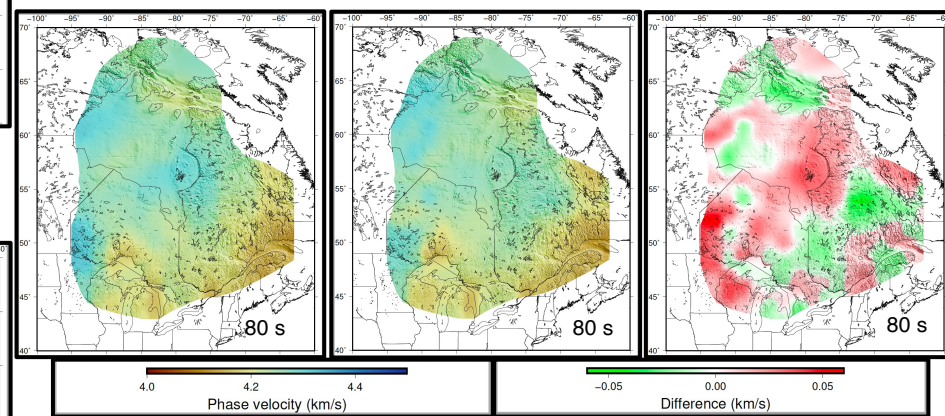


❖ Predicted data are depicted as the means of their respective posterior PDFs

Observed

Predicted

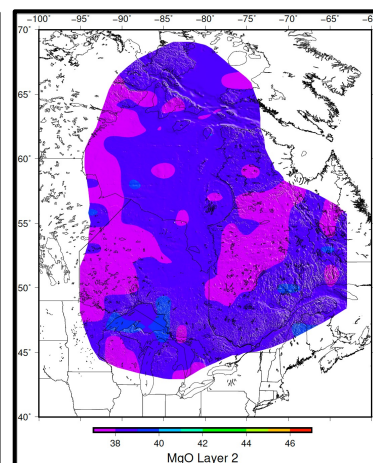
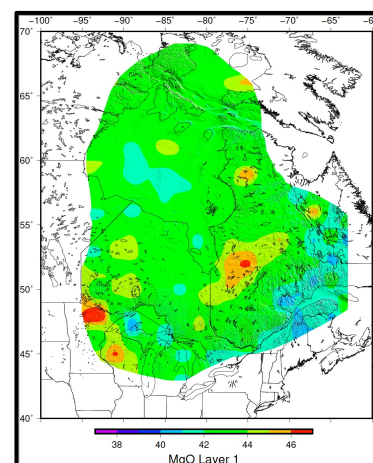
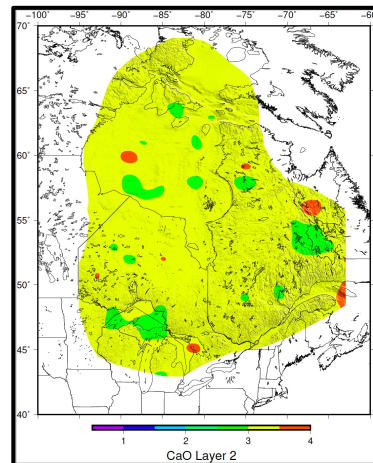
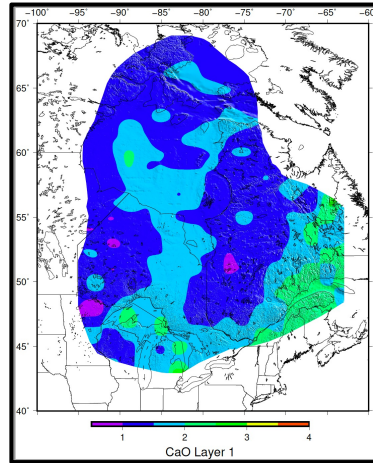
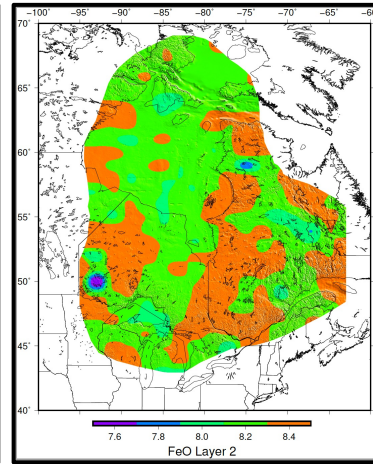
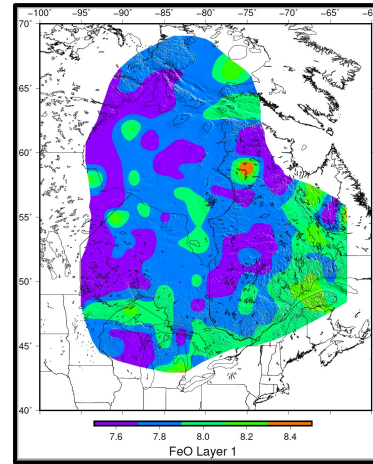
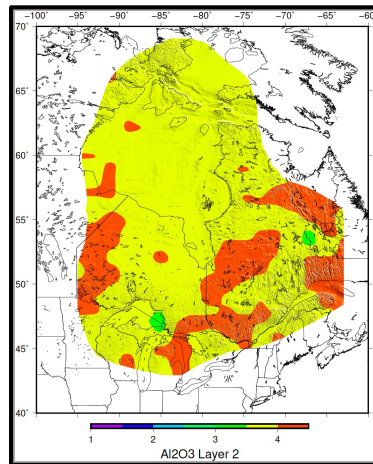
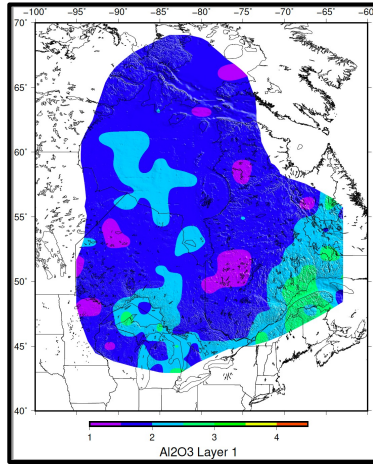
Difference



❖ The fit to dispersion data remains within uncertainties in most of the study area

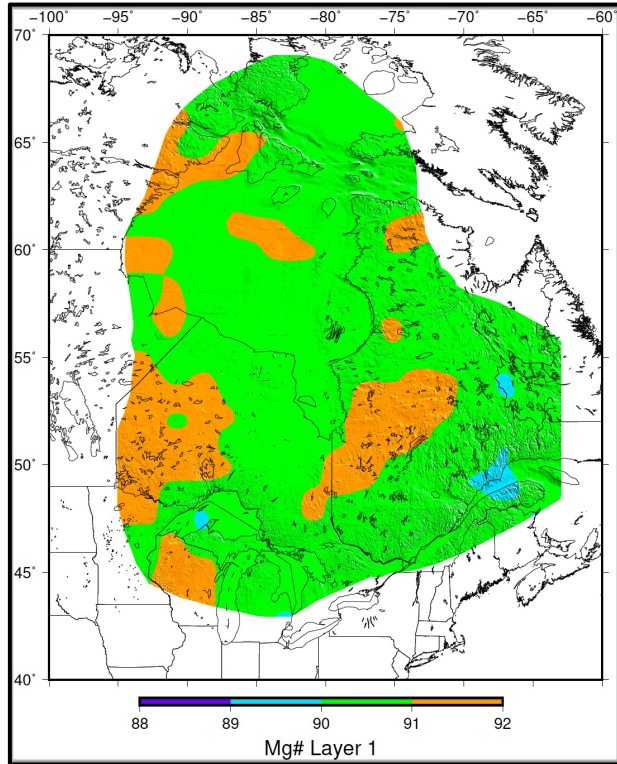
Upper Mantle Compositions

Layer 1 = Lithosphere, Layer 2 = Sub-lithosphere

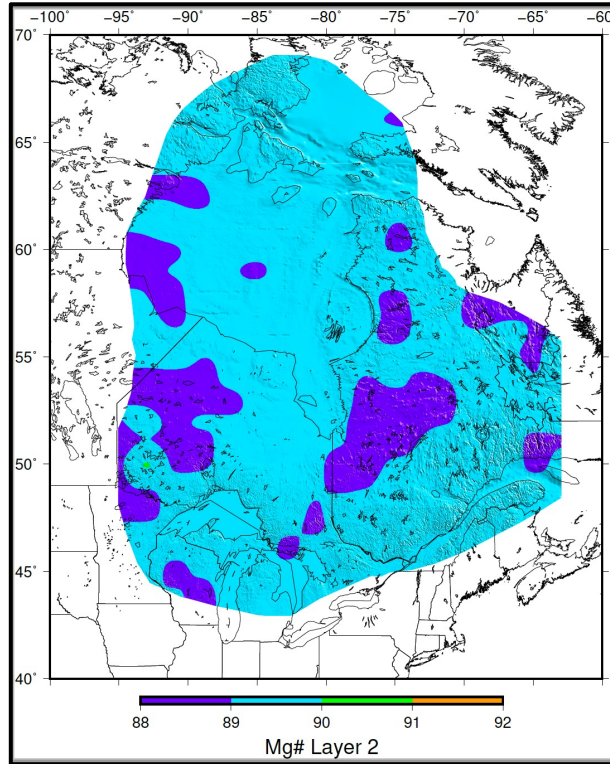


Upper Mantle Compositions

Lithosphere

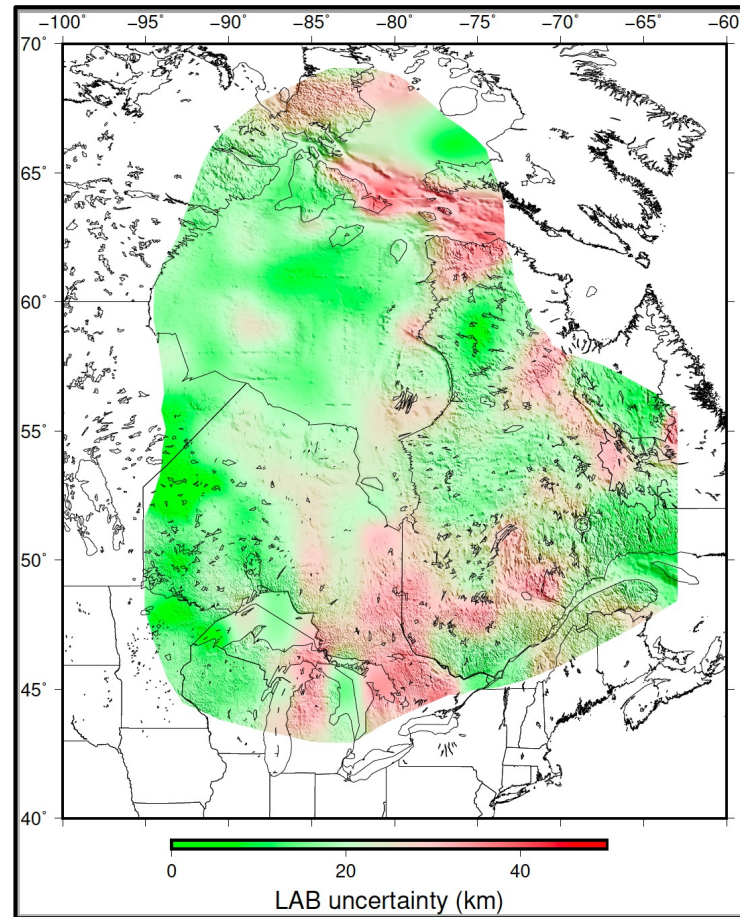
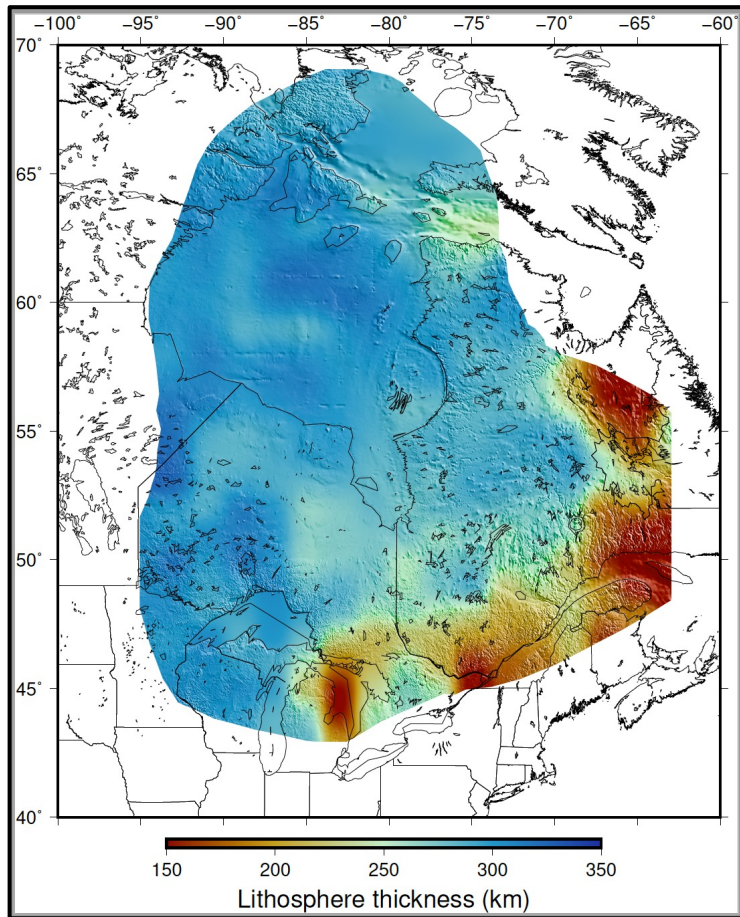


Sub-lithosphere



- ❖ Magnesium Number:
$$\text{Mg\#} = \frac{(\text{Mg}/40.30)}{((\text{Mg}/40.30) + (\text{Fe}/71.84))} * 100$$
- ❖ High Mg# (>90) – refractory, depleted mantle
- ❖ Low Mg# (<90) – fertile or refertilized mantle
- ❖ Lithosphere (Layer 1) is more depleted than sub-lithosphere (Layer 2)

LAB Depths and Uncertainties



- ❖ Integration of V_p data in the inversion
- ❖ Further tests for the appraisal of various parameters
- ❖ Possibility of adding Mid-Lithospheric Discontinuities (MLDs) if the data demands
- ❖ Opportunity for comparison of model LAB depths (and thus geotherms) with xenolith constraints
- ❖ Refinement in 3D inversion to yield compositional and thermal structure of the lithosphere and upper mantle

